Journal of Colloid and Interface Science 349 (2010) 408–416

Contents lists available at ScienceDirect

Journal of Colloid and Interface Science

www.elsevier.com/locate/jcis

Evolution of volume fractions and droplet sizes by analysis of electrical conductance curves during destabilization of oil-in-water emulsions

M. Kostoglou, E.-M. Varka, E.P. Kalogianni [1], T.D. Karapantsios *

Division of Chemical Technology, School of Chemistry, Aristotle University of Thessaloniki, Univ. Box 116, 541 24 Thessaloniki, Greece

ARTICLE INFO

Article history:
Received 9 March 2010
Accepted 8 May 2010
Available online 16 May 2010

Keywords:
Emulsions
Destabilization
Electrical conductance technique
Droplet size distribution
Droplet motion

ABSTRACT

Destabilization of hexane-in-water emulsions is studied by a continuous, non-intrusive, multi-probe, electrical conductance technique. Emulsions made of different oil fractions and surfactant ($C_{10}E_5$) concentrations are prepared in a stirred vessel using a Rushton turbine to break and agitate droplets. During the separation of phases, electrical signals from pairs of ring electrodes mounted at different heights onto the vessel wall, are recorded. The evolution of the local water volume fractions at the locations of the electrodes is estimated from these signals. It is found that in the absence of coalescence, the water fraction evolution curve from the bottom pair of electrodes is compatible with a bidisperse oil droplet size distribution. The sizes and volume fractions of the two droplet modes are estimated using theoretical arguments. The electrically determined droplet sizes are compared to data from microscopy image analysis. Results are discussed in detail.

1. Introduction

Emulsion stability is one of the most important factors governing the shelf life of foods, pharmaceuticals, cosmetics, etc. Principally, emulsions are dispersed, multiphase systems consisting of at least two insoluble liquids [1]. Emulsions are thermodynamically unstable due to unfavorable contact between oil and water molecules [2], and consequently their physical structures tend to change over time by various mechanisms such as creaming, flocculation, coalescence, and Ostwald ripening, eventually leading to complete phase separation.

Stability over time is usually achieved by the addition of an emulsifier which is often a surfactant. Emulsifiers facilitate the formation of emulsions and improve their stability by reducing the oil–water interfacial tensions and by forming a protective layer around droplets to prevent coalescence [3]. Nevertheless, surfactants may not be able to provide sufficient long-term stability to the emulsions against flocculation which leads to the instability of the systems.

Several methods have been employed in the past e.g. optical microscopy, laser diffraction, light scattering, etc. to investigate the progress of emulsion's destabilization, which determine droplet sizes either from direct visual observations or from measurements performed on withdrawn samples [4–10]. These methods are limited by the fact that they provide information of droplet sizes only from places where there is either visual access or a sampling mechanism can be inserted. Sampling can alter the emulsion characteristics by exerting forces that can disturb seriously the phases distribution. Additionally, the often required significant dilution of samples before measurement can modify some of the emulsion characteristics (e.g. destroy flocks or aggregates). Moreover, these methods cannot provide information on local phase concentrations.

Electrical techniques appear to be a tempting option for measuring non-intrusively the temporal evolution of local volume fractions inside emulsions (opaque or transparent). Such techniques have been used in the past for monitoring other applications such as mixing [11], bubble columns [12], multiphase flows [13,14], solid–liquid filtration [15], and polymerization reactors [16]. In those studies different electrode geometries and possibilities to arrange/configure electrodes have been employed. A pair of ring electrodes running the internal circumference of a vessel and separated by a certain distance in the axial direction constitutes a probe which, apart from being non-intrusive, is particularly sensitive to phase distribution patterns in the cylindrical segment between the ring electrodes [17]. Ring electrodes have been successfully applied to a number of multi phase applications e.g. [18–21]. It has been reported that in cases of radially homogeneous dispersions the separation distance between electrodes can be significantly reduced in favor of more localized (axially) measurements.

To our knowledge there has been no systematic use of electrical measurements for studying the evolution of local volume fractions during emulsion's destabilization. Some papers used conductance measurements more as an indicator of global emulsion condition

* Corresponding author. Fax: +30 2310 99 7772.
E-mail address: karapant@chem.auth.gr (T.D. Karapantsios).
[1] Present address: Department of Food Technology, Technological Educational Institution, Thessaloniki, PO Box 14561, 541 01 Thessaloniki, Greece.

0021-9797/$ - see front matter © 2010 Elsevier Inc. All rights reserved.
doi:10.1016/j.jcis.2010.05.032

rather than as a tool for determining local volume fractions [20–22]. The aim of this work is to examine the application of a non-intrusive, on-line, electrical conductance technique for monitoring the evolution of local phase volume fractions inside opaque oil-in-water emulsions during destabilization. Multiple ring electrodes located at different axial locations of the container register variations along the height of the emulsion in a tomographic fashion. Lately, this version of the electrical technique was used in our lab for monitoring the progress of emulsification (production of emulsions) of the same oil/water mixtures inside the same stirred vessel [22].

In this work, a new analysis is detailed for estimating droplet sizes from the evolution of electrical signals measured during destabilization. Only signals obtained near the bottom of the container are presently exploited since only there certain simplifying assumptions hold. It remains for the future to expand the analysis to signals from any part of the emulsion. Recently, results from electrical signals measured near the bottom of a small container were compared with global volumetric measurements and microscopy photos obtained during the destabilization of Pickering emulsions [23]. Despite some limitations when using very high particles concentration, which appear to affect the viscosity of the continuous phase, results on droplet sizes and phase separation were considerably successful.

Emulsification of hexane-in-water mixtures is performed using pentaethyleneglycol monodecyl ether ($C_{10}E_5$) as emulsifier. $C_{10}E_5$ is a non-ionic surfactant belonging to the *n*-alkyl polyethyleneglycol ethers (C_iE_j) group of surfactants. These surfactants are broadly used as emulsifiers in applications such as tertiary oil recovery, medicine, cosmetics, nanoscience and analytical chemistry [24–26]. In addition, hexane/water/$C_{10}E_5$ emulsions are chosen for emulsification studies in the FASTER facility of the International Space Station, under a European Space Agency project (FASES: Fundamental and Applied Studies of Emulsion Stability) where the present authors are actively involved [27].

The structure of the present work is as follows: First the experimental procedure is described in detail. Then, experimental electrical signals are presented and their relevance to the emulsion stability is discussed. The theoretical background and methodology for the derivation of droplet sizes from electrical conductance curves are described next. The electrically estimated droplet sizes are compared to those resulting from optical microscopy. Finally, the dependence of droplet sizes on emulsification parameters and the discrepancies in the estimated statistical averages between different measurement techniques are extensively discussed.

2. Materials and methods

2.1. Materials

Oil-in-water emulsions were prepared using a NaCl aqueous solution, *n*-hexane and $C_{10}E_5$ as emulsifier. The aqueous solution was prepared by dissolving NaCl at a concentration of 50 mg/L into Millipore filtered water. After salt dissolution the electrical conductivity of the aqueous solution was 125 μS/cm, a value typical of tap water. It must be stressed, though, that the present electrical technique is fully functional even down to ~10 μS/cm aqueous solution conductivity. Hexane was spectroscopy grade (purity ⩾98.5%, Uvasol, Merck). Three different oil-to-water volume ratios: 40/60, 20/80, 5/95 were used for making emulsions. The emulsifier, $C_{10}E_5$ (Nikko Chemicals Ltd.), was initially dissolved in water but once in contact with hexane during emulsification it started dissolving into hexane and partitioned between the two phases. The partition coefficient of $C_{10}E_5$ between water and hexane is Kp = 13.9 [28]. To achieve the same final $C_{10}E_5$ concentration when increasing the hexane/water volume ratio, higher initial surfactant concentrations in water have been employed. The concentration of $C_{10}E_5$ initially dissolved in water and the final -concentration after partitioning are displayed in Table 1 for all experiments. With only exception the case 5/95 hexane-in-water and final concentration $C_f = 10^{-4}$ M, all other cases have initial surfactant concentrations, C_i, above the CMC [22].

2.2. Emulsification procedures and microscopy measurements

Emulsification was conducted inside a cylindrical Plexiglas vessel having 19.5 cm height and 7 cm internal diameter. The vessel was furnished with 16 stainless steel ring electrodes flush mounted to the inner wall, 1.5 cm apart from each other. Electrodes combined in pairs provide several non-intrusive conductance probes. Electrical signals from multiple probes combined with a multiplexer and a suitable inverse reconstruction algorithm for data reduction constitute a tomographic imaging system [29]. As this was an attempt to employ tomographic measurements to emulsification, tests were initially conducted with signals taken from all possible views of the sensing electrodes. Due to the intense mixing during emulsification virtually no angular or radial variations of volume fractions were found but only variations in the axial direction [22]. To ease the computational effort and increase data acquisition rate, only three probes at different axial locations along the vessel were eventually employed, designated for convenience as *high*, *middle* and *low* (Fig. 1). These probes consisted of adjacent electrodes which offered certain advantages: the 1.5 cm separation distance between rings was large enough to average droplet size undulations yet small enough to prevent the local character of measurements. All probes were located at the lower half of the emulsion, 1, 4 and 7 cm, respectively, from the bottom of the vessel (distances calculated from the center of probes). The free surface of the emulsion was 16 cm above the bottom of the vessel (total liquid volume 616 ml).

Table 1
Concentration of $C_{10}E_5$ in the water phase at the beginning of emulsification (C_i) and final concentration of $C_{10}E_5$ after partitioning (C_f) at the different hexane concentrations (Φ) used for emulsion preparation.

Φ (v/v) %	5	20	40
C_f (M)	C_i (M)		
10^{-4}	1.7×10^{-4}	4.5×10^{-4}	1.0×10^{-3}
2×10^{-4}	3.5×10^{-4}	8.9×10^{-4}	2.0×10^{-3}
5×10^{-4}	8.6×10^{-4}	2.2×10^{-3}	5.1×10^{-3}
10^{-3}	1.7×10^{-3}	4.4×10^{-3}	1.0×10^{-2}

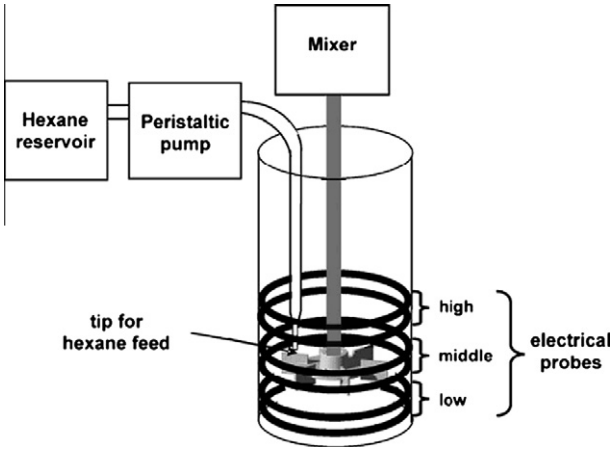

Fig. 1. Schematic representation of the employed experimental set-up.

Emulsification was implemented by intense mixing of water and oil using an impeller (Rushton turbine, $d = 4.6$ cm) placed at the central axis of the vessel. The impeller was placed 1.7 cm above the bottom of the vessel. High shearing rates and intense mixing which are necessary for producing fine oil droplets characterized the hydrodynamic conditions in the region close to the impeller blades. Emulsification started by feeding the hexane at a steady flow rate of 0.5 ml/s under continuous agitation at 290 rpm with the help of a peristaltic pump (Watson Marlow, Falmouth, Cornwall TR114RU) at a location 2 mm above the impeller blades. After running 8 min at 290 rpm the impeller was adjusted to 750 rpm and was left to run for 10 additional minutes and then it was switched-off. Experiments were conducted in triplicates at 22 ± 1 °C. Reproducibility was satisfactory along the whole electrical curves obtained during emulsification and destabilization with an average variance of 0.1 among runs.

Right after switching-off the impeller, a 0.5 ml sample was carefully withdrawn from the vessel (from the center of the *low* probe) using a 5 mm i.d. tube (wide enough to prevent droplets jamming) and was added to a 20% w/v Tween 80 solution to prevent droplets coalescence. The sample was put under a microscope (AxionStar) which was coupled with a digital camera (SONY DSC-F717 CYBER-SHOT 5.0 megapixels) where several photos were taken until reaching a population of droplets above 300 to ensure statistical significance in the determination of droplets size. A custom-made software [30] was employed to obtain droplet size distributions (Fig. 2) and from them calculate basic statistical quantities of droplet size.

2.3. Electrical conductance measurements

Electrical conductance data were taken throughout the emulsions destabilization process, simultaneously from all three probes. The technique has been presented in detail elsewhere [20], only a few essential elements are repeated here. An a.c. carrier voltage of 0.250 V_{RMS} was applied across each electrode pair at a frequency of 25 kHz. This frequency allows suppressing undesirable electrode polarization and capacitive impedance. The response of each probe was fed to an electronic analyzer–demodulator. The analog d.c. output signal of the analyzer from the different probes was acquired at a rate of 1 Hz with the aid of a data acquisition card (ADAM 4018, Advantec) interfaced to a PC. The acquired d.c. signals were then converted to apparent conductance K_{app} (the inverse of apparent resistance) of the emulsion using a calibration curve based on precision resistors. Assuming a uniform dispersion of oil-in-water inside the measuring volume of each probe, the following holds:

$$\left(\frac{K_{dis}^{app}}{K_{aq}^{app}}\right) = \frac{\sigma_{dis}}{\sigma_{aq}} \tag{1}$$

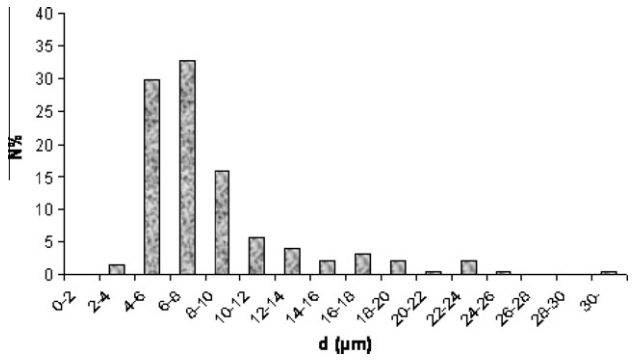

Fig. 2. Particle size distribution of 20/80 1×10^{-4} M emulsion.

where K_{dis}^{app} and σ_{dis} denote the apparent conductance and conductivity of the dispersion whereas K_{aq}^{app} and σ_{aq} denote the apparent conductance and conductivity of the aqueous phase. The normalization of conductance measurements with respect to the conductance of the aqueous phase eliminates errors owing to variations of liquid conductivity. The normalized conductivity measurements were then transformed into water fraction (φ_w) measurements using the equation of Bruggeman which is quite popular for emulsion applications, e.g. [22,31]

$$\sigma_{dis} = \sigma_{aq}(\varphi_w)^{3/2} \tag{2}$$

3. Results and discussion

3.1. Electrical signals during emulsions destabilization

Figs. 3–5 present electrical measurements of local water volume fraction obtained by the three probes (*high*, *middle*, *low*) during the destabilization process of hexane-in-water emulsions at different $C_{10}E_5$ concentrations. Fig. 3a–d display data for 5/95 (v/v) emulsions, Fig. 4a–d for 20/80 (v/v) emulsions and Fig. 5a–d for 40/60 (v/v) emulsions. The mentioned v/v proportions are those at the end of hexane addition.

Electrical signals from all runs exhibit common features. Time $t = 0$ is the moment that the impeller is switched-off which corresponds to a well-mixed homogeneous emulsion along the test vessel [22]. This means that signals from the three probes start from the same initial water volume fraction which for the three examined oil/water proportions is 0.95, 0.80 or 0.60, respectively. At long times, electrical curves of water fraction tend to unity which corresponds to presence of water alone. This is because all three probes are located at the lower half of the emulsion volume so at the end of phase separation electrodes are covered only by water. In all curves, a fast rise is observed at the beginning which progressively turns into a slower rise at longer times. The initial fast rise corresponds to large oil droplets that separate rapidly from the aqueous phase whereas the slow rise corresponds to small droplets that take longer to destabilize. In the next section it will be shown that the existence of two main slopes in the shape of the water volume fraction curves implies an approximately bi-disperse size distribution of droplets.

The initial fast slopes of the *low* probe are steeper than of the other two probes. There are two possible explanations for this. First, oil droplets departing from the bottom of the container are not replaced by other droplets, whereas, on the contrary, for the middle and high probes there are droplets coming from below. Second, as droplets raise to higher locations in the vessel their concentration increases and this hampers their movement. This is manifested at the first segment of the curves of the *middle* and *higher* probes where there is a short inception period during which the water fraction slightly drops or stays constant. The possibility cannot be excluded that this effect still exists (but gradually less) also in the subsequent parts of the curves where there is a net increase of water fraction. As the surfactant concentration increases this feature lasts longer reflecting the more stable conditions in the emulsion.

The enhanced stability with denser surfactant concentrations explains also why the initial slopes from all probes get smaller as surfactant concentration increases. A higher surfactant concentration affects strongly the interfacial tension and interfacial elasticity [22] yielding smaller and harder to coalesce droplets. This is more pronounced for concentrations above 2×10^{-4}. Fig. 6 show electrical curves for all the examined surfactant concentrations for the 5/95 and 20/80 v/v oil/water mixtures and only from the *low* probe. Only these particular curves are analyzed in the subsequent

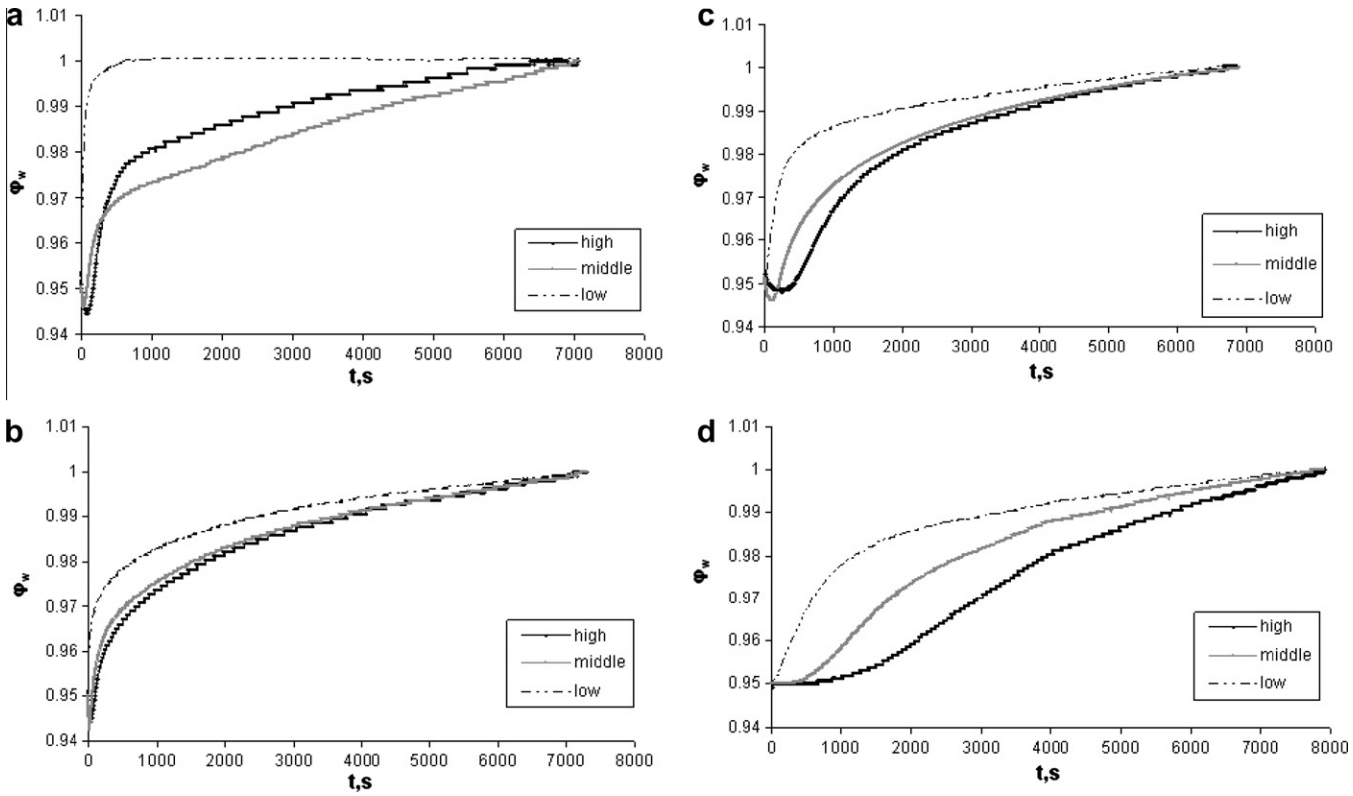

Fig. 3. Water fraction (φ_w) as a function of time (t) during destabilization of a hexane-in-water emulsion at a 5/95(v/v) (final proportion) oil/water volume ratio. Figures (a–d) present emulsions with different emulsifier concentrations. In (a) $C_f = 1 \times 10^{-4}$ M, (b) $C_f = 2 \times 10^{-4}$ M, (c) $C_f = 5 \times 10^{-4}$ M and (d) $C_f = 1 \times 10^{-3}$ M where C_f is the concentration of surfactant after partitioning between the two phases.

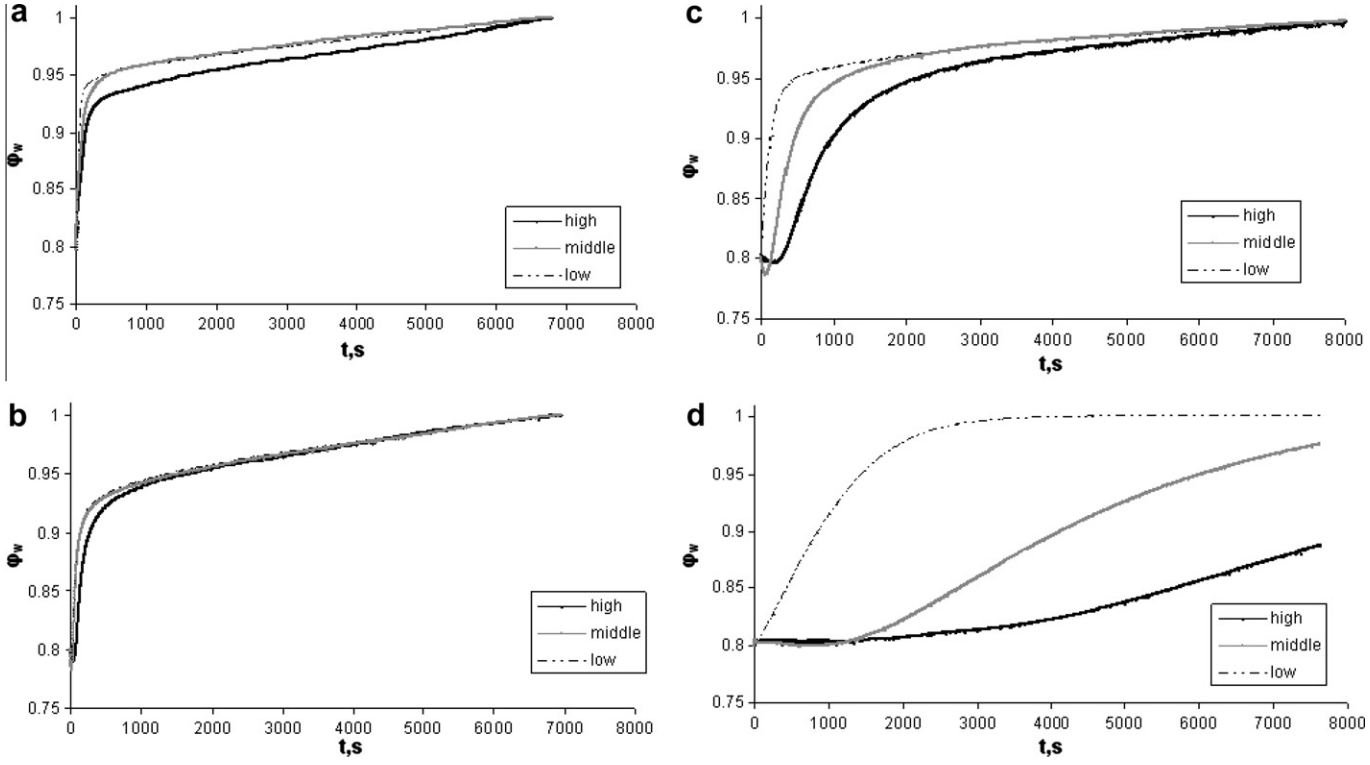

Fig. 4. Water fraction (φ_w) as a function of time (t) during destabilization of a hexane-in-water emulsion at a 20/80(v/v) (final proportion) oil/water volume ratio. Figures (a–d) present emulsions with different emulsifier concentrations. In (a) $C_f = 1 \times 10^{-4}$ M, (b) $C_f = 2 \times 10^{-4}$ M, (c) $C_f = 5 \times 10^{-4}$ M and (d) $C_f = 1 \times 10^{-3}$ M where C_f is the concentration of surfactant after partitioning between the two phases.

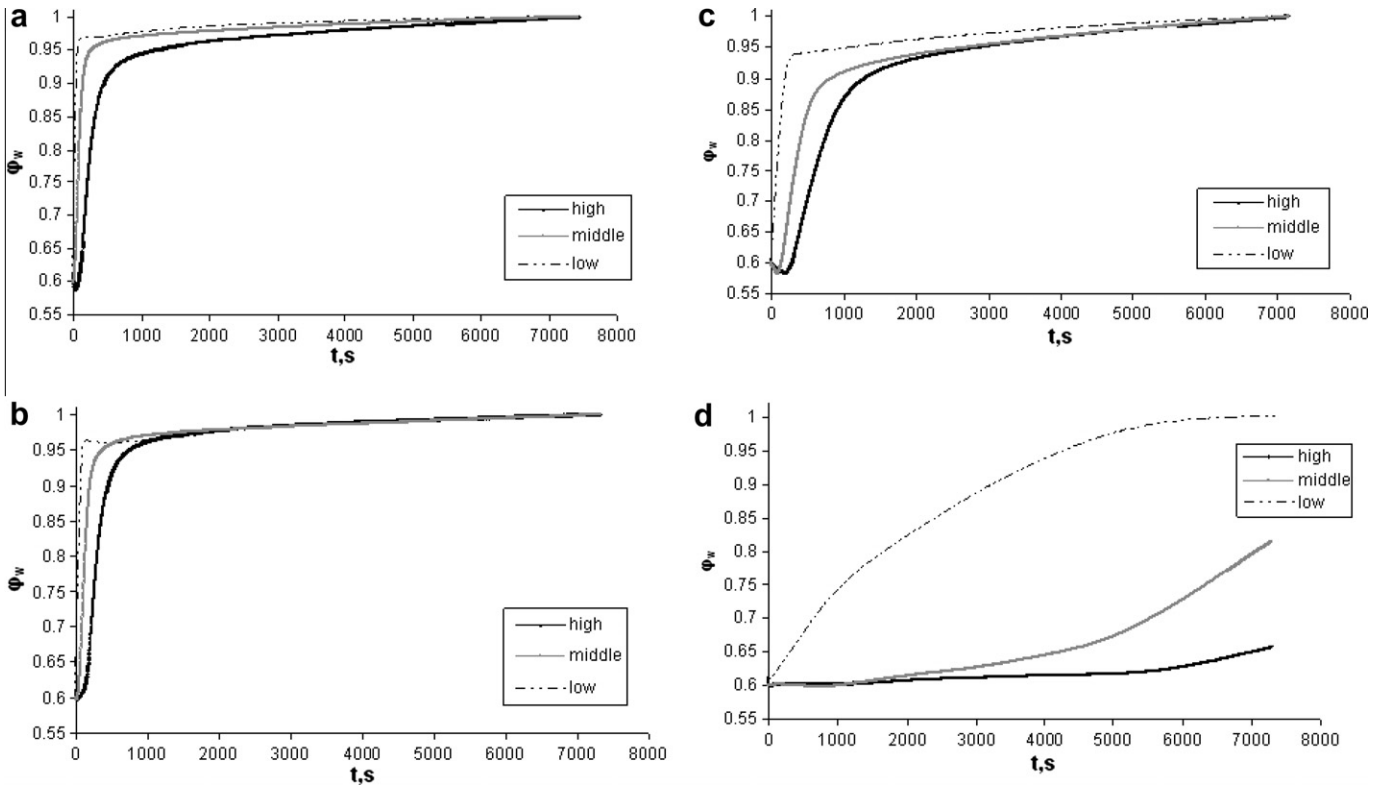

Fig. 5. Water fraction (φ_w) as a function of time (t) during destabilization of a hexane-in-water emulsion at a 40/60(v/v) (final proportion) oil/water volume ratio. Figures (a–d) present emulsions with different emulsifier concentrations. In (a) $C_f = 1 \times 10^{-4}$ M, (b) $C_f = 2 \times 10^{-4}$ M, (c) $C_f = 5 \times 10^{-4}$ M and (d) $C_f = 1 \times 10^{-3}$ M where C_f is the concentration of surfactant after partitioning between the two phases.

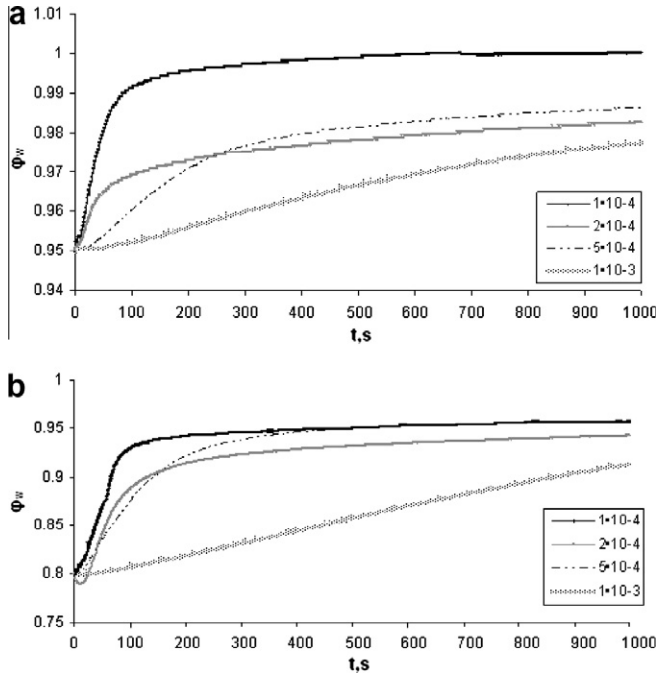

Fig. 6. Water fraction (f_w) as a function of time (t) during emulsification for all surfactant concentrations for (a) 5/95 and (b) 20/80 v/v oil/water mixtures from the low probe.

section for droplet size determination. This is because in the 40/60 v/v mixtures oil droplets are so densely populated that practically touch each other so the concept of emulsion destabilization by their buoyant free flow is not valid. Instead, destabilization in the latter case passes through different stages of droplets rearrangement. It must be stressed that Figs. 3–5, although not utilized for droplet size determination, are extremely valuable in presenting the evolution of the local water fraction at different heights of the test vessel. This information covers a major part of the present objective to provide a tomographic-type of measurement of volume fraction distribution during emulsion destabilization.

Equally safe arguments can not be made with respect to the later slow rising section of the electrical curves associated with smaller droplets in the emulsion. The ambiguity regarding these droplets is not because of difficulties in measuring accurately the signal but because it is just a simplification to assume a distinct constant value for the small slope in the curves which actually looks more like a progressively converging slope. This converging slope corresponds to a broad distribution of small droplets which dominates the late stages of destabilization and dictates the time for water fraction to become unity. Apparently, minor differences in the distribution of small droplets can lead to appreciably different total duration of destabilization.

3.2. Theoretical analysis of electrical signals for droplet size determination

The detailed model of the destabilization procedure is very complex. The buoyancy velocity of each bubble is influenced from its neighboring bubbles. In addition to this motion, diffusion occurs (especially for small bubbles) simultaneously with coalescence due to gravitational motion and to Brownian motion. The theory of each from the above phenomena (influenced by several parameters) is incomplete, leaving many open issues to be resolved based on experimental results. In addition, the computational cost of such a model is rather large to be used for extensive parameter

identification by fitting the model to experimental data. Such a model was formulated in [32] in which empirical parameters were added to the theoretical models in order to achieve matching with experimental droplet size distributions. Due to the computational cost of the problem the unknown parameters were found by inspection and not through a deviation minimization technique. The development of a pressure build-up [33] in the suspension of dense non-coalescing particles makes the modeling procedure even more complicated.

An alternative direct approach to extract problem parameters from experimental data is developed here. The shape of the evolving water volume fraction curve for the *low* measuring probe (Fig. 6) implies a bi-disperse size distribution of droplets. The term bidisperse literally refers to a population with two discrete sizes. Nevertheless, in practice, it is a good approximation for any bimodal distribution with no very broad modes and with limited overlapping between modes. This is apparently the case here since the distinct character of the two modes is clear in the experimental conductance curves (see below). The development procedure to estimate droplet sizes and relative volume fractions from the experimental data of the *low* probe is described next.

The first issue is the relation between the conductance measurements and the composition of the dispersion. In general, the Laplace equation with mixed boundary conditions (Dirichlet on the electrodes and Neumann on the non-conducting material) and with an electrical conductivity undergoing a spatial dependence due to the spatial distribution of the oil volume fraction, must be solved numerically. The numerical solution of the problem requires a very fine discretization to capture the singularity that arises from the discontinuity of the boundary conditions at the edges of the electrodes. This numerical solution must be repeated at each time step to construct the conductance–time curve having known the spatiotemporal evolution of the oil fraction in the dispersion.

In order to develop a simple technique for the estimation of droplets size from the corresponding volume fraction evolution curve, the very simple case of a moving front separating two phases with oil contents φ_1 and φ_2 is considered first. Let's assume that the "measuring" volume is contained between the centers of the two electrodes comprising a measuring probe. For simplicity, the two electrodes are designated as lower/upper reflecting their relative position along the test vessel. The distance between the centers of the two electrodes is denoted L (see Fig. 7). The motion of the front is to the upper direction which implies that $\varphi_2 > \varphi_1$. The instantaneous distance between the front and the center of the lower/upper electrode is x_1/x_2, respectively, such as $x_1 + x_2 = L$. Instead of solving the complete electrostatic problem based on the Laplace equation for the electrostatic potential, it is assumed that two resistances in series with conductivities given by the Bruggeman law as $k_1 = k_w(1-\varphi_1)^{3/2}$ and $k_2 = k_w(1-\varphi_2)^{3/2}$ are contained between the electrodes. The average conductivity k of the medium contained in the observation volume will be given according to the resistances in series model as:

$$k = \left(\frac{x_1}{k_1 L} + \frac{x_2}{k_2 L}\right)^{-1} \tag{1}$$

Inverting the procedure followed to create the experimental φ vs. t curves based on the Bruggeman equation leads to the following relation for φ:

$$\varphi = 1 - \left(\frac{x_1}{(1-\varphi_1)^{3/2} L} + \frac{L - x_1}{(1-\varphi_2)^{3/2} L}\right)^{-2/3} \tag{2}$$

Assuming a constant velocity U of the front motion and an initial position $x = 0$ at an arbitrary time value t_o, the evolution equation for φ takes the form (t_o does not influence the analysis):

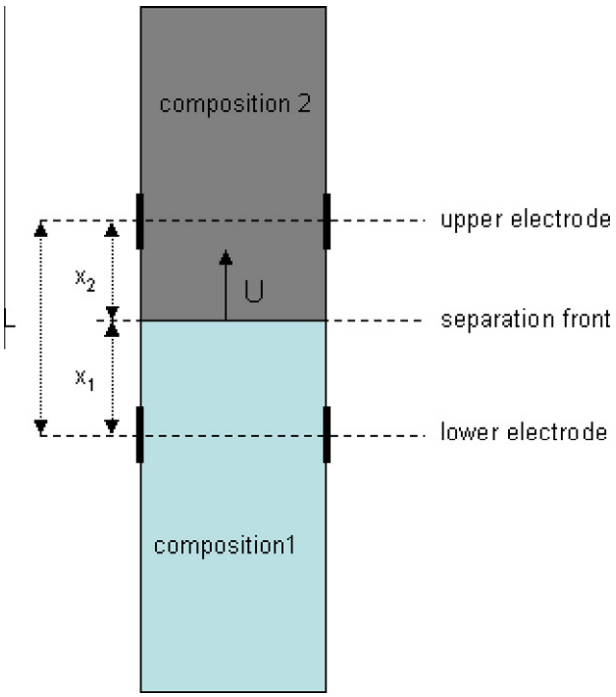

Fig. 7. Schematic and notation of the motion of the front separating two regions with different oil concentration.

$$\varphi = 1 - \left(\frac{1}{(1-\varphi_2)^{3/2}} + \frac{U(t-t_o)}{L}\left(\frac{1}{(1-\varphi_1)^{3/2}} - \frac{1}{(1-\varphi_2)^{3/2}}\right)\right)^{-2/3} \tag{3}$$

The second term in the parenthesis is in general smaller than the first term so expanding the power term in Taylor series and keeping only the first term leads to:

$$\varphi = \varphi_2 - (1-\varphi_2)\frac{2Ut}{3L}\left(1 - \left(\frac{1-\varphi_2}{1-\varphi_1}\right)\right)^{3/2} \tag{4}$$

Differentiating the above equation with respect to time and solving for the front velocity U, the following expression relating the front velocity to the curve $\varphi(t)$ and to the characteristics of the phases separated by the front is derived:

$$U = -\frac{d\varphi}{dt}\frac{3L}{2(1-\varphi_2)}\left(1 - \left(\frac{1-\varphi_2}{1-\varphi_1}\right)^{3/2}\right) \tag{5}$$

It is reminded here that the function φ is not the spatial distribution of the oil fraction but it is a purely experimental time-depended function resulting by applying Bruggeman law to the conductance signals.

Assuming that the droplet population consists of n discrete droplet sizes $d_1, d_2, \ldots, d_n$ in order of increasing size, n fronts appear. The jth front separates a phase with droplet sizes d_1, d_2, d_{j-1} from a phase with sizes d_1, $d_2, \ldots, d_j$ and according to the above analysis (provided that only one front at each moment is between the electrodes) the $\varphi(t)$ curve should be consisted of n linear pieces with different slopes. The curves from the *low* probe in Fig. 6 exhibit two main slopes implying that the droplet size distribution can be approximated by a bidisperse one. Now assuming a bidisperse distribution with small droplets with diameter d_s and volume fraction φ_s and large droplets with diameter d_L and volume fraction φ_L, one can estimate the velocity U_1 of the front separating the initial dispersion from the dispersion containing only small particles and the velocity U_2 of the front separating the dispersion containing small particles from pure water as (where $\varphi_w = 1 - \varphi$):

$$U_1 = \left(\frac{d\varphi_w}{dt}\right)_1 \frac{3L}{2(1-\varphi_s-\varphi_L)}\left(1-\left(\frac{1-\varphi_s-\varphi_L}{1-\varphi_s}\right)^{3/2}\right) \quad (6)$$

$$U_2 = \left(\frac{d\varphi_w}{dt}\right)_2 \frac{3L}{2(1-\varphi_s)}(1-(1-\varphi_s)^{3/2}) \quad (7)$$

The subscripts 1 and 2 at the derivatives indicate the slope of the first and the second linear part of the experimental $\varphi_w(t)$ curves (see Fig. 8 for an example of their estimation from the experimental curves). In practice there is no slope discontinuity at the intersection of the linear parts of the curve as the above theory predicts but a smooth transition from one part to the other. This is mainly due to the (ignored by the simplified model) sensitivity of the measured conductance to the front position when it is not between the electrodes. The two distinct slopes identified in Fig. 8 highlight the implied bidispersity of the droplet size distribution.

The procedure to find the velocities U_1, U_2 and the oil volume fractions φ_L, φ_s from an experimental curve is the following: At first, tangential lines at the two "linear" parts of the curve are drawn and their intersection point corresponding to a water content φ_c is found (Fig. 8). Then the volume fractions of the two oil components are computed as $\varphi_s = 1-\varphi_c$ and $\varphi_L = \Phi - \varphi_s$, respectively, where Φ is the nominal oil volume fraction of the dispersion. Finally, the corresponding velocities U_1 and U_2 are computed from the relations (6) and (7) using the slopes of the two tangential curves.

The next step is to relate the front velocities U_1 and U_2 to the corresponding droplet sizes d_L and d_s, a problem being in the core of the sedimentation theory. According to the general theories of polydisperse sedimentation [34] the velocity of each species (droplet size) depends on the velocity of the other species. This interdependence of the two droplet sizes velocities can be ignored here since (i) regarding the first front, the small droplet velocity is very small to influence the velocity of large droplets and (ii) the second front occurs in the absence of the large droplets. So, the oil volume fraction for the first front is considered to be Φ and for the second front to be φ_s.

What remains is to find a relation for the buoyancy velocity of a droplet at a specified dispersed phase volume fraction. Although a first thought could be the Hadamard–Rybczynski relation [35], i.e. the extension of Stokes law for mobile interfaces, the situation is more complicated regarding the following three factors. The first factor is the mobility of the fluid–fluid interface. In practice, the interface can vary from completely mobile (in the absence of surfactant) to completely immobile (if enough surfactant is present). In principle, the influence of surfactant to the drag coefficient (and therefore to the buoyancy velocity) can be found from the solution of a very complicated hydrodynamic-mass transfer problem [36]. Fortunately, the saturation with respect to surfactant occurs at low concentrations so for the present experiments the surfactant concentrations ensure that the fluid–fluid interface is immobile (similar to solid–liquid one).

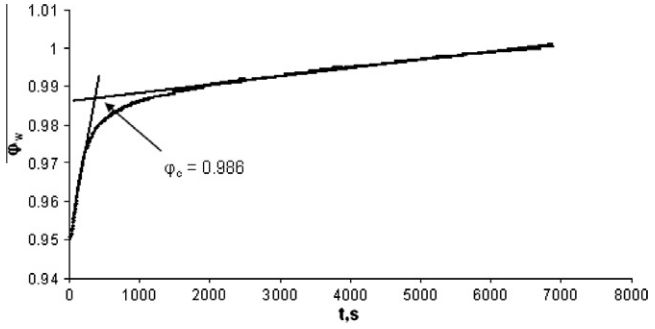

Fig. 8. The procedure followed in order to calculate the two slopes and the transition point φ_c.

The second factor is the existence of a finite volume fraction of the dispersed phase. This effect has been extensively studied in literature using several means from asymptotic calculations from disordered [37] and ordered [38] structures to numerical solutions for ordered structures [39], approximate approaches such as the well known Happel and Kuwabara cells [40] and, finally, empirical relations [41]. The empirical relation of Richardson and Zaki was found the most successful in correlating experimental results. It is just a correction of the form $(1-\varphi)^n$ to the drag force relation, where n is the so-called Richardson–Zaki exponent. In many situations this empirical correlation is compatible to the theoretical expressions (for example $n = 6.5$ according to low φ theory in [37]) but the value of n differs from experiment to experiment. It is a function of the single droplets Reynolds number (based not on their real velocity but on that of an isolated droplet) and a correlation for this dependence is $n = (1.791 + 0.133\mathrm{Re}^{0.456})/(0.359 + 0.093\mathrm{Re}^{0.456})$ [42]. Of course, this approach can be used only for approximate computations as it is the case here since the correlation for the exponent is not the only one (see for example [43]) and moreover there is a large scatter in the exponent values found by fitting different experimental results.

The third factor is the non-zero Reynolds number. Fortunately, in the present experiments the single droplet Re number is always smaller than 1 so the Oseen correction to the Stokes drag law can be applied. Unifying the immobility of the interface, the Richardson–Zaki approach to the hindering effect of the oil volume fraction and the Oseen correction to the Stokes law yields the following relation for the buoyancy velocity (u is the single droplet velocity and it is used in the computation of Re).

$$u = \frac{(\rho_w - \rho_{oil})gd^2}{18\mu} \quad (8)$$

$$U = u(1+3\mathrm{Re}/16)(1-\varphi)^{(1.791+0.133\mathrm{Re}^{0.456})/(0.359+0.093\mathrm{Re}^{0.456})} \quad (9)$$

where μ is the water viscosity, ρ_w, ρ_o are the water and oil density, respectively and d is the droplet diameter. Replacing the velocity values from the experimental results and the corresponding oil fractions for each velocity, the large and small droplet diameters d_L and d_s can be estimated.

Applying the above analysis to the experimental curves in Fig. 6, allows estimation of the volume fractions and the average diameters for the bidisperse droplet size distribution for each experiment. It is noted that the computed size distributions from the *low* probe are not compatible with the data taken from the other two probes (*middle*, *high*) implying that more complex phenomena than simple front motion occurs between electrodes.

The results of the analysis are shown in Table 2. The two droplet size modes appear to have very different values which is compatible with the way of producing the emulsions in the present work. The oil is introduced from a capillary to an intensively stirred tank. The initial large droplets leaving the capillary undergo turbulent breakage (the existence of surfactant prevents coalescence both in the emulsification and the destabilization stage). It is well known that in case of intensive turbulence breakage occurs by dripping tiny droplets from the surface of mother droplets [44,45]. This type of breakage leads to a bimodal distribution. The large mode corresponds to the continuously decreasing size of the initial droplets and the small mode to the fragments. The above mechanism is imposed by surface energy and capillary pressure criteria [44,45]. Further to the expected bimodal shape, it is evident from Table 2 that the size of the large mode decreases as the surfactant concentration increases. This is explained by the fact that the reduction of surface energy leads to higher breakage rate and thus to larger

Table 2
Results from the theoretical analysis of electrical data from the lower electrode ring based on the assumption of a bidisperse droplet size distribution: bubble diameters d_L and d_s with oil volume fractions φ_L and φ_s respectively. D_{opt} is the number average diameter from the optical measurements.

Concentration of $C_{10}E_5$ (M)	Hexane %(v/v)	φ_L	d_L (μm)	φ_s	d_s (μm)	D_{opt} (μm)
1×10^{-4}	5	0.042	88.3	0.008	10	17.74
2×10^{-4}	5	0.034	74.8	0.016	9.62	30.58
5×10^{-4}	5	0.036	39.2	0.014	9.56	22.86
1×10^{-3}	5	0.033	21.8	0.017	8.3	15.78
1×10^{-4}	20	0.155	126	0.045	10.7	8.6
2×10^{-4}	20	0.14	123	0.06	15	13.64
5×10^{-4}	20	0.147	85.2	0.053	9.38	25.93
1×10^{-3}	20	0.2	27	0	–	27.68

breakage extent. Finally, the higher large mode size for larger oil volume fraction probably is due to the well-known damping of turbulence by the presence of the dispersed phase. For very high breakage extent the breakage mechanism changes from dripping to equal size breakage leading to the merging of the two modes to one [44,45]. This seems to be the case for the 20/80 v/v mixture with 10^{-3} surfactant concentration in which the second mode vanishes.

3.3. Significance of different statistical averages

Interestingly, the droplet size distributions computed from microscopy measurements are unimodal with a number average droplet size sometimes closer to the large size mode and some times closer to the small size mode estimated from electrical measurements (see D_{opt} in last column of Table 2). In order to explain this discrepancy let us consider what exactly is measured by each technique. The number density concentration of the droplets is denoted as $f(d)$ and its moments as $M_i = \int_0^\infty d^i f(d) dd$. Let us also define that $D_{i,j} = (M_i/M_j)^{1/(i-j)}$. The characteristic droplet size calculated from microscopy data is $D_{1,0} = M_1/M_0$ whereas the characteristic droplet size calculated from electrical data is the $D_{5,3}$ (given that the latter is sensitive to volume fractions and the droplet velocity depends on the second power of the droplet size). In general, several average diameters can be defined for different i and j values. The most common is the Sauter diameter $D_{3,2}$ and the volume weighted average diameter $D_{4,3}$ (often used in emulsion stability studies [32]). For a monodisperse size distribution all the average diameters coincide but as the spread of the distribution increases, the deviation among them increases, too. As an example, the aforementioned four average diameters for a bidisperse distribution with equal volume fraction of droplet sizes d_2 and d_1 are shown versus the ratio d_2/d_1 between the sizes in Fig. 9. The $D_{3,2}$ is closer to $D_{1,0}$ whereas $D_{4,3}$ is closer to $D_{5,3}$. As the size ratio d_2/d_1 increases, the two diameter $D_{5,3}$ and $D_{1,0}$ can differ from each other by almost an order of magnitude.

The effect of the volume fraction θ of the large droplets ($1-\theta$ is the volume fraction of the small droplets) for $d_2/d_1 = 5$ is shown in Fig. 10. It is apparent that $D_{1,0}$ exhibits small sensitivity with respect to large droplets. It is actually dominated by small droplets regardless their presence in a small quantity. But if the above is the case for a bidisperse distribution, what is the case for a smooth broad unimodal distribution like those determined by microscopy measurements (Fig. 2). In Fig. 11 the same four average diameters are shown for a distribution having a log-normal shape which is typical for fitting droplet size experimental data. It is surprising that $D_{5,3}$ is virtually outside the region of droplet sizes covered by the distribution. This is why one should not expect any relevance between the optically derived distributions and the size estimation of the electrical technique. In the above example, the emulsion stability (as depicted by electrical conductance curves) depends on large droplets which constitute the ~1/10,000 of the total droplets number. This means that optical monitoring of the emulsion is highly improbable to observe even a single large droplet of that size even in images containing 1000 droplets. This is even worse if one considers that such large droplets move fast and easily escape from the optical field of view. It is stressed here that as the droplet size distribution becomes narrower the averages $D_{1,0}$ and $D_{5,3}$ approach each other so the optical measurements and the electrical conductance technique predictions for the average size are compatible. Generating relatively narrow unimodal droplet size distributions (e.g. by a combined coales-

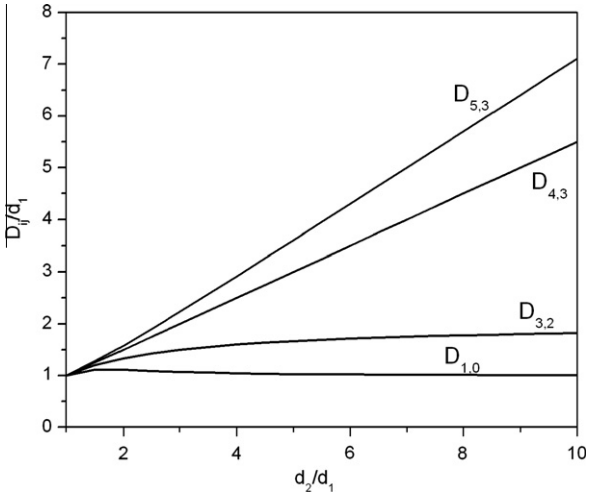

Fig. 9. Normalized average diameters vs. size ratio for bidisperse droplet size distribution with volume fraction of droplets having sizes d_1 and d_2.

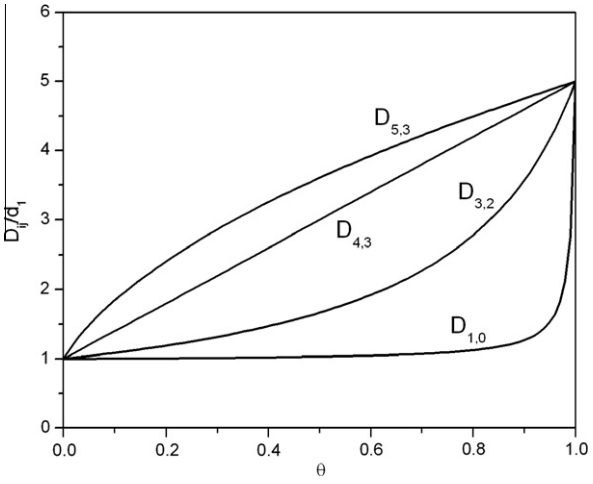

Fig. 10. Normalized average diameters vs. volume fraction of large droplets θ for bidisperse droplet size distribution with $d_2/d_1 = 5$.

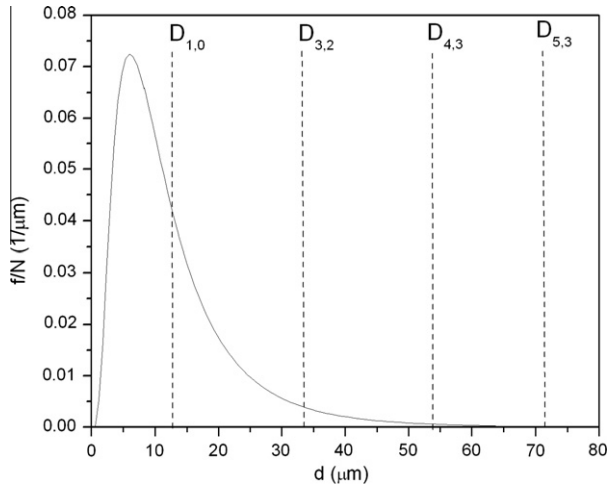

Fig. 11. Normalized number density droplet distribution f/N is the total droplet concentration of a log-normal shape. Several average diameters are also show.

cence-breakage process instead of the pure breakage process of the present work) will give the opportunity to cross-validate the size measurement techniques.

The electrical technique which assess directly the stability of an emulsion has the capability to split a highly disparate bimodal size distribution to its components and give the $D_{5,3}$ diameter for each one of them as it is described in the present work (a global $D_{5,3}$ would be quite insensitive to the smaller droplets mode). Of course, any of the above four average diameters can be easily calculated from higher order moments of the experimental data. Yet, the above discussion (and depending on the spread of the distribution) shows that only the average diameter linked with the physical mechanism of a measuring technique is correct. Therefore, the droplet sizes measured by microscopy are less related to emulsion stability compared to those measured by the electrical conductance technique. Both techniques give complementary information about the droplet size distribution, apparently with no appreciable degree of overlapping, especially, for the broad size distributions usually arising from the emulsification procedure.

4. Conclusions

The employed electrical conductance technique was capable of registering non-intrusively the variation of water fraction during destabilization of hexane-in-water emulsions with $C_{10}E_5$ as emulsifier. The use of multiple sensing probes provided accurate measurements of local water fractions at different heights along the test vessel. In addition, with appropriate theoretical treatment the conductance curves obtained near the bottom of the test vessel can be used to estimate the two characteristic droplet sizes of an assumed bimodal distribution. These sizes are quite different from those measured directly by an optical microscopy. The difference can be explained by the fact that the two techniques are based on very different mechanisms to estimate droplet average size. It was shown that the droplet sizes estimated by the electrical conductance technique are much more representative of the emulsion stability than the one estimated by direct optical observation.

Acknowledgments

Financial support by the European Space Agency through the project FASES (Fundamental and Applied Studies of Emulsion Stability) (ESA-AO-2004-PCP-109/ELIPS-2) is gratefully acknowledged. This work was conducted under the umbrella of the COST P21 action: Physics of Droplets.

References

[1] J. Sjoblom, Emulsions and Emulsions Stability, vol. 61, Marcel Dekker, New York, 1996.
[2] S.E. Friberg, Emulsion stability, in: S.E. Friberg, K. Larsson (Eds.), Food Emulsions, vol. 1–55, Marcel Dekker, New York, 1997.
[3] M.J. Rosen, Surfactants and Interfacial Phenomena, John Wiley & Sons, New York, 1978.
[4] T. Förster, M. Waldmann-Laue, W. Both, C. Jassoy, Int. J. Cosmet. Sci. 21 (4) (1999) 253–264.
[5] M.C. Sanchez, M. Berjano, A. Guerrero, C. Gallegos, Langmuir 17 (18) (2001) 5410–5416.
[6] T. Goloub, R.J. Pugh, J. Colloid Interface Sci. 257 (2003) 337–343.
[7] C. Desnoyer, O. Masbernat, C. Gourdon, Chem. Eng. Sci. 58 (7) (2003) 1353–1363.
[8] M.M.M. Ribeiro, M.M.L. Guimaraes, C.M.N. Madureira, J.J.C. Cruz Pinto, Chem. Eng. J. 97 (2) (2004) 173–182.
[9] S. Sajjadi, Langmuir 22 (13) (2006) 5597–5603.
[10] D. Clausse, F. Gomez, I. Pezron, L. Komunjer, C. Dalmazzone, Adv. Colloid Interface Sci. 117 (1–3) (2005) 59–74.
[11] L. Pakzad, F. Ein-Mozzafari, P. Chan, Chem. Eng. Sci. 63 (9) (2008) 2508–2522.
[12] E. Fransolet, M. Crine, P. Marchot, D. Toye, Chem. Eng. Sci. 60 (22) (2005) 6118–6123.
[13] G.P. Lucas, J. Cory, R.C. Waterfall, W.W. Loh, F.J. Dickin, Flow Meas. Instrum. 10 (1999) 249–258.
[14] F. Ricard, C. Brechtelsbauer, X.Y. Xu, C.J. Lawrence, Chem. Eng. Res. Des. 83 (7) (2005) 794–805.
[15] D. Vlaev, M. Wang, T. Dyakowski, R. Mann, B.D. Grieve, Chem. Eng. J. 77 (1–2) (2000) 87–91.
[16] M. Kaminoyama, S. Taguchi, R. Misumi, K. Nishi, Chem. Eng. Sci. 60 (20) (2005) 5513–5518.
[17] N.A. Tsochatzidis, T.D. Karapantsios, M.V. Kostoglou, A.J. Karabelas, Int. J. Multiphase Flow 18 (1992) 653–667.
[18] T.D. Karapantsios, N.A. Tsochatzidis, A.J. Karabelas, Chem. Eng. Sci. 48 (8) (1993) 1427–1436.
[19] T.D. Karapantsios, E.P. Sakonidou, S.N. Raphaelides, Carbohydr. Polym. 49 (4) (2002) 479–490.
[20] T.D. Karapantsios, M. Papara, Colloids Surf., A: Physicochem. Eng. Asp. 323 (1–3) (2008) 139–148.
[21] M. Papara, X. Zabulis, T.D. Karapantsios, Chem. Eng. Sci. 64 (2009) 1404–1415.
[22] E.P. Kalogianni, E.-M. Varka, T.D. Karapantsios, M. Kostoglou, E. Santini, L. Liggieri, F. Ravera, Colloids Surf., A: Physicochem. Eng. Aspects 354 (2010) 353–363.
[23] E-M. Varka, C. Ampatzidis, M. Kostoglou, T.D. Karapantsios, V. Dutschk, Colloids Surf., A: Physicochem. Eng. Asp., 2010, accepted for publication.
[24] C. Browarzik, D. Browarzik, Fluid Phase Equilib. 235 (2005) 127–138.
[25] A. Berthod, S. Tomer, J.G. Dorsey, Talanta 55 (2001) 69–83.
[26] D. Niegowski, M. Hedren, P. Nordlund, S. Eshaghi, Int. J. Biol. Macromol. 39 (2006) 83–87.
[27] R. Miller, D. Grigoriev, J. Kragel, A.V. Makievski, V.B. Fainerman, V.I. Kovalchuk, L. Liggieri, F. Ravera, M. Ferrari, E. Santini, G. Loglio, V. Dutschk, T.D. Karapantsios, Project proposal for the investigation of particle-stabilised emulsions and foams by microgravity experiments, Microgravity Sci. Technol. XVIII (3/4) (2006) 104–107.
[28] M. Ferrari, L. Liggieri, R. Miller, F. Ravera, Prog. Colloid Polym. Sci. 115 (2000) 222–226.
[29] V. Papoti, S. Deirmentzoglou, T.D. Karapantsios, G. Doxastakis, P. Mavros, Design of electrical resistance tomography probes for foam and emulsion stability measurements, in: International Workshop on Bubble and Drop Interfaces 2004, Bubbles and Drops 2004, Genova, April 25th–28th, 2004.
[30] X. Zabulis, M. Papara, A. Chatziargyriou, T.D. Karapantsios, Colloids Surf., A: Physicochem. Eng. Asp. 309 (2007) 96–106.
[31] M. Rondón-González, L.F. Madariaga, V. Sadtler, L. Choplin, L. Márquez, J-L. Salager, Ind. Eng. Chem. Res. 46 (2007) 3595–3601.
[32] R. Cunha, M. Fortuny, C. Dariva, A.F. Santos, Ind. Eng. Chem. Res. 47 (2008) 7094–7103.
[33] T.D. Dimitrova, T.D. Gurkov, N. Vassileva, B. Campbell, R.B. Borwankar, J. Colloid Interface Sci. 230 (2000) 254–267.
[34] S. Berres, R. Burger, E.M. Torry, Chem. Eng. J. 111 (2005) 105–117.
[35] W. Rybczynski, Bull. Acad. Sci. Cracow Ser. A (1911) 40.
[36] R.S. Subramanian, R. Balasubramaniam, The Motion of Bubbles and Drops in Reduced Gravity, Cambridge University Press, New York, 2001.
[37] G.K. Batchelor, J. Fluid Mech. 52 (1972) 245–268.
[38] D.L. Koch, A.S. Sangani, J. Fluid Mech. 400 (1999) 229–263.
[39] D.L. Koch, R.J. Hill, Annu. Rev. Fluid Mech. 33 (2001) 619–647.
[40] J. Happel, H. Brenner, Low Reynolds Number: Hydrodynamics with Special Applications to Particulate Media, New York, 1973.
[41] J.F. Richardson, W.N. Zaki, Trans. Inst. Chem. Eng. 32 (1954) 35–41.
[42] A.V. Nguyen, H.J. Schulze, Colloidal Science of Flotation, Marcel Dekker, New York, 2004.
[43] E.E. Michaelides, Particles, Bubbles, Drops, Their Motion, Heat and Mass Transfer, World Scientific, Singapore, 2006.
[44] T. Wang, J. Wang, J. Jin, Chem. Eng. Sci. 58 (2003) 4629–4637.
[45] M. Kostoglou, A.J. Karabelas, Chem. Eng. Sci. 60 (2005) 6584–6595.